

Defect Trapping and Phase Separation in Chemically Doped Bulk AgF_2

Adam Grzelak,* Mariana Derzsi, and Wojciech Grochala*

Cite This: *Inorg. Chem.* 2021, 60, 1561–1570

Read Online

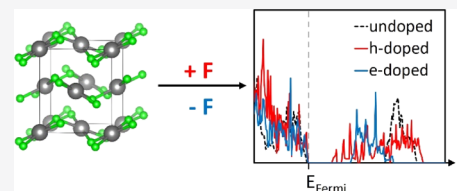
ACCESS |

Metrics & More

Article Recommendations

Supporting Information

ABSTRACT: We report a computational survey of chemical doping of silver(II) fluoride, which has recently attracted attention as an analogue of La_2CuO_4 —a known precursor of high-temperature superconductors. By introducing fluorine defects (vacancies or interstitial adatoms) into the crystal structure, we obtain nonstoichiometric, electron- and hole-doped polymorphs of $\text{AgF}_{2\pm x}$. We find that the ground-state solutions show a strong tendency for localization of defects and of the associated electronic states, and the resulting doped phases exhibit insulating or semiconducting properties. Furthermore, the distribution of Ag(I)/Ag(III) sites which appear in the crystal structure points to the propensity of the AgF_2 system for phase separation upon chemical doping, which is in line with observations from previous experimental attempts. Overall, our results indicate that chemical modification may not be a feasible way to achieve doping in bulk silver(II) fluoride, which is considered essential for the emergence of high- T_c superconductivity.



INTRODUCTION

Silver(II) fluoride has recently attracted attention of chemists and physicists alike because of its similarities to precursors of copper oxide-based superconductors.^{1–3} Charge doping within their constituent Cu–O₂ layers is a key step toward achievement of superconductivity in cuprates.⁴ Given the aforementioned similarities, it is justified that doping of AgF_2 should also be studied.

Charge doping of a compound can be achieved experimentally by several different means. For example, using a field-effect transistor setup, it is possible to alter the concentration of charge carriers to the desired degree and produce materials with modified electronic and magnetic properties.⁵ At the computational level, this can be simulated, for example, by explicitly setting the number of electrons in the unit cell to a number that differs from the sum of all valence electrons of its constituent atoms. This has already been attempted by our group in bulk AgF_2 and in hypothetical monolayers.⁶ The latter, although as yet unknown, could in principle be obtained by epitaxy.⁷ Another approach is to synthesize a material with a modified (e.g., nonstoichiometric) composition, leading to mixed (or intermediate) valence of one of its constituent elements. That is the case with copper oxide-based superconductors: for example, in La_2CuO_4 , the first known precursor to high-temperature superconductors, a substitution of a fraction of La(III) cations for, for example, Ba(II)⁸ or an increase of nonmetal content⁹ leads to hole doping of Cu–O layers. Computationally, this can be easily modeled by inserting, removing, or substituting certain atoms in the studied unit cell. In this contribution, we utilize a similar approach. By changing the number of F atoms in the AgF_2 unit cell, we obtain different levels of charge doping and analyze crystal, electronic, and magnetic structures of the resulting

polymorphs. This in turn enables us to assess the prospect for cuprate-like properties in these materials.

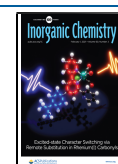
COMPUTATIONAL METHODS

All calculations were performed with the density functional theory (DFT) approach as implemented in VASP software^{10–14} using the GGA-type Perdew–Burke–Ernzerhof functional adapted for solids (PBEsol).¹⁵ A plane-wave cutoff energy of 520 eV was used. A k -point mesh of $2 \times 2 \times 2$ (spacing of ca. $0.04 \text{ } 2\pi \text{ \AA}^{-1}$) was used for structural optimization and $4 \times 4 \times 4$ (spacing of ca. $0.02 \text{ } 2\pi \text{ \AA}^{-1}$) for total energy and electronic density of states (eDOS) calculations. The energy threshold for convergence was 10^{-5} eV for the ionic cycle and 10^{-7} eV for the electronic cycle. For spin-polarized calculations, on-site Coulombic interactions of Ag d electrons were accounted for through DFT + U correction as introduced by Liechtenstein et al.,¹⁶ with the Hubbard U and Hund J_H parameters for Ag set to 5 and 1 eV, respectively.¹⁷ VESTA software was used for visualization of crystal structures.¹⁸ eDOS was plotted with p4vasp software.¹⁹

Because we describe here the defective unit cells with either F vacancies or adatoms, one should in principle use large unit cells to prevent intercell electrostatic repulsion between defects;²⁰ fortunately, our studies have shown that vacancies tend to strongly cluster around one Ag site, and thus these are the intracell Coulombic effects which predominate defect–defect interactions rather than the intercell ones. The supercell dimension used here is a reasonable compromise between the tendency to minimize intercell interactions and limited resources we had.

Received: October 6, 2020

Published: January 19, 2021



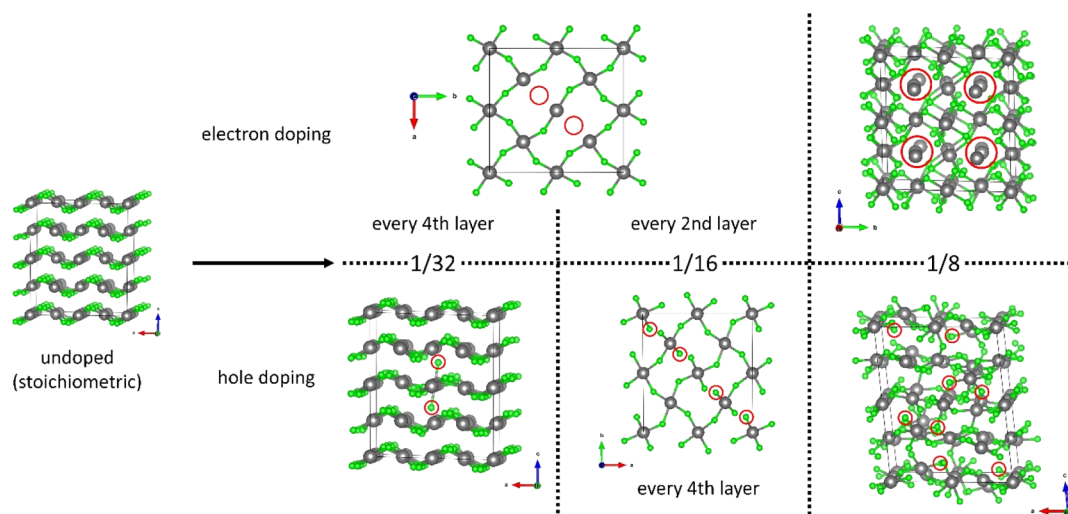


Figure 1. Structures of modified AgF_2 supercells. Fractions represent the doping level. Red circles indicate vacancies and interstitials for electron and hole doping, respectively. “Every n -th layer” indicates that this pattern appears in $4/n$ out of 4 layers in the unit cell. For e-doped 1/32 and 1/16 solutions, the same pattern is pictured, but it appears in the said solutions every fourth and every second layer, respectively. For e-doped 1/8 solution, the emptied local environment of several Ag atoms is highlighted instead for clarity.

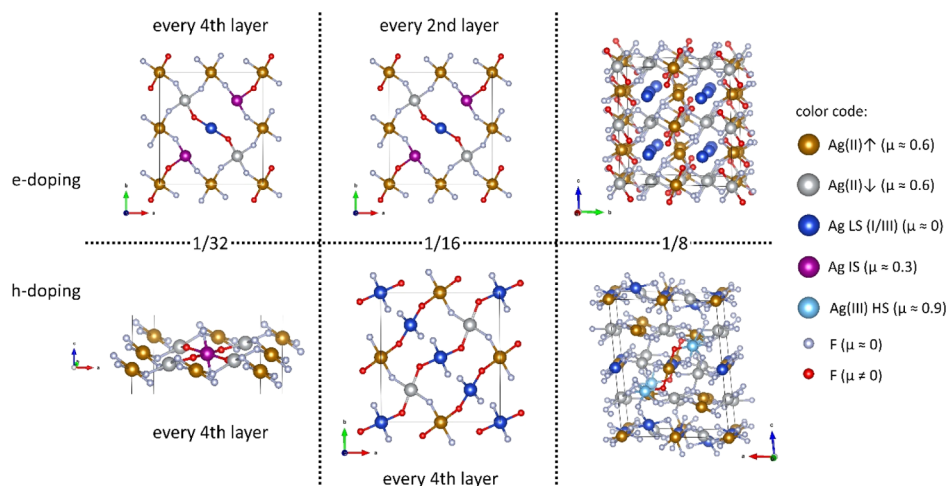


Figure 2. Magnetic ordering in ground-state doped AgF_2 solutions. Fractions represent the doping level. “ μ ” refers to magnetic moment in units of μ_B . LS—low spin, HS—high spin, IS—intermediate spin. “Every n -th layer” indicates that this pattern appears in $4/n$ out of 4 layers in the unit cell.

The value of $U = 5$ eV used in this study has been suggested in many previous theoretical studies (e.g., Kasinathan et al.¹⁷), and it has been successfully used to predict crystal structures of high-pressure polymorphs of AgF_2 .²¹ In order to verify appropriateness of the methodology used here for description of a diluted antiferromagnetic (AFM) Mott insulator, we have varied the value of U up to 6.5 eV; the outcome proved rather insensitive to the U value (cf. Section S2 of Supporting Information). In addition, we have carried out similar calculations for the e^- - and h^+ -doped La_2CuO_4 , and we have observed similar formation of mid-gap states as those seen for the title compounds in the e^- -doped case and facile metallization in the h^+ -doped one (cf. Section S3 of Supporting Information).

RESULTS AND DISCUSSION

Crystal and Magnetic Structure. It should be noted that AgF_2 , although similar in many ways to La_2CuO_4 ,¹ is a binary [001] compound, which greatly reduces the number of ways its stoichiometry can be modified, as compared to ternary La_2CuO_4 . Our starting point was a $2 \times 2 \times 2$ supercell of silver(II) fluoride (which crystallizes in a $Pbca$ orthorhombic structure²²) containing 32 formula units (FU) of AgF_2 , pre-

optimized using the GGA + U approach described in the previous section (cf. Section S10 of Supporting Information). We then modified the supercell by removing or adding fluorine atoms into the structure, which led to electron or hole doping, respectively.

We only studied supercells with modified F content, as opposed to Ag content, because of practical considerations: it is chemically more feasible to manipulate the content of lighter, more mobile F atoms in order to alter the composition of AgF_2 . Experimentally, this corresponds to controlled thermal decomposition (e^- -doping) or fluorination (h^+ -doping). Fluorine deficiency has also been found to occur in laser-illuminated samples of AgF_2 during Raman spectroscopy analyses.¹ On top of that, our preliminary computational analysis shows that Ag defects have a higher energy cost than F defects: ca. 2 times for interstitials and by a few percent for vacancies. Therefore, we decided that the scheme of removing or adding F atoms is the best way to systematically assess energetic effects of doping.

We investigated three doping levels on each side of the phase diagram: 1/32, 1/16, and 1/8, which correspond to

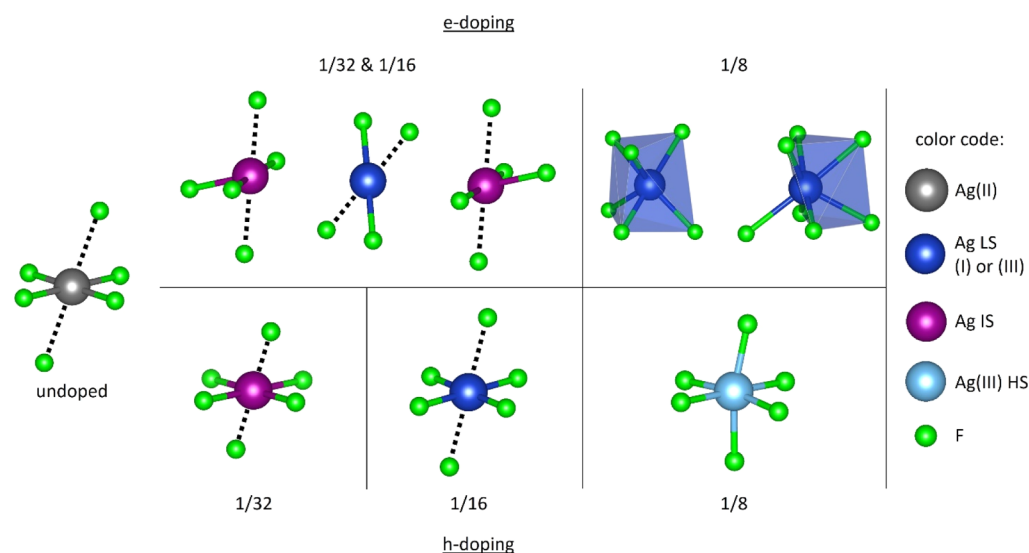


Figure 3. Comparison of local coordination of an Ag(II) site in undoped AgF_2 and of Ag(I) and Ag(III) sites in doped solutions. LS—low spin, HS—high spin, IS—intermediate spin.

removal/addition of 2, 4, and 8 F atoms, respectively, compared to the starting supercell. The optimization of modified supercells was carried out in two steps. In the first step, the structures were optimized at the GGA level, without Hubbard correction or magnetic interactions. After that, magnetic models were constructed in pre-optimized structures, taking into account changes in local coordination of Ag sites and intuitions from Goodenough–Kanamori–Anderson rules.²³ These magnetic models were taken as the starting point for optimization at the GGA + U level, with spin polarization and Hubbard correction described in the previous section. Several possible patterns of removal/addition of F atoms were studied at each doping level; all of these patterns preserved the inversion center of the unit cell, which we consider a reasonable compromise between flexibility of geometry optimization and use of computational resources. Only the lowest-energy solutions are presented and discussed in this work. Their structures are shown in Figure 1. (cf. Section S1 of Supporting Information for coordinates of removed/added F atoms in input structures that led to the most stable solutions.)

The ground-state structure of bulk stoichiometric AgF_2 consists of layers stacked along the c dimension of the unit cell. The most stable solutions of doped AgF_2 investigated in this work exhibit some common features, which point to overall tendencies associated with doping. The lowest-energy solutions of 1/32 and 1/16 e-doped models are both characteristic of the same pattern of F vacancies aligned along the ab diagonal of the unit cell, only in the 1/16 solution, the pattern is repeated every two layers along the c direction and shifted by (0.5, 0.5) in the ab plane every other instance. Also, in the hole-doped solutions at 1/32 and 1/16 levels, the defects—in this case additional F atoms—are localized around a single Ag site or contained within a single layer. In contrast, at the 1/8 level, a more complex, three-dimensional pattern emerges in both e-doped and h-doped solutions.

In order to understand the influence of fluorine vacancies and interstitials, we have to take a closer look at their magnetic structure, which is shown in Figure 2. Additional information can be inferred from spin density maps plotted in Section S4 in Supporting Information. In bulk AgF_2 (not shown), each layer

within the ab plane features two-dimensional AFM ordering of spins on Ag(II) sites (with a magnetic moment of ca. $0.57 \mu_B$, as obtained with the GGA + U approach). In the first approximation and assuming localization of additional charge, the number of new Ag(I) cations in e-doped solutions should be equal to the number of F vacancies (conversely, the same applies to the number of Ag(III) cations and F interstitials in h-doped solutions). We find it to be true for solutions at the 1/8 doping level. In e-doping, Ag(I) cations are located in channels along the a directions within a three-dimensional framework of AgF_2 . There is also a lot of additional spin (ca. $0.10 \mu_B$) on dangling F atoms, that is, those connected only to one Ag(II) cation; magnetic moments of this size are in fact typical for fluoroconnections of Ag(II).²⁴ Ag(I)–F contacts are not shown for clarity, but they are also substantially longer than Ag(II)–F: 2.3–2.6 Å compared to 2.0–2.1 Å (more detailed description of local coordination will be presented below). In h-doped 1/8 solution, there are eight clearly discernible Ag(III) sites: two of high-spin d^8 electronic configuration—with a high magnetic moment (ca. $0.86 \mu_B$) and roughly octahedral coordination—and six of low-spin configuration, with null magnetic moment and roughly square-planar coordination. The spin density map shows that the latter type of Ag(III) sites in this solution exhibits spin polarization on both $d(x^2 - y^2)$ and $d(z^2)$ orbitals, which further supports their high-spin character.

In e-doped solutions at 1/32 and 1/16 levels, there is a clearly discernible Ag(I) site ($\mu = 0$) in the middle of the defect pattern, with two additional Ag sites of intermediate spin [$0.30 \mu_B$, i.e., between null and the value typical for regular Ag(II)], which we also designated as contributing to Ag(I) states in their electronic structure (discussed in the corresponding section later in the text). The spin density map shows a dumbbell-shaped distribution of magnetic moment on these intermediate-spin sites, which is likely a result of hybridization between empty 5s and occupied 4d(z^2) orbitals. The two intermediate-spin Ag sites are equivalent by symmetry. Therefore, such distribution of spin can be considered a superposition of two solutions, in either of which a second Ag(I) cation occupies only one of those two positions. We re-optimized the 1/32 e-doped model with unit

Table 1. Comparison of Local Coordination Spheres of Ag Sites for Undoped, e-Doped, and h-Doped AgF_2 ^a

model	coordination		
undoped AgF_2	Ag(II) —4 + 2		
	2.069 (square)		
	2.570 (axial)		
e-doped	Ag(I) —2 + 2†	Ag IS —3 + 2†	Ag(I) —6(+1)
	2.151 (linear)	2.189 (in-plane)	2.443 (trigonal prism/monocapped)
	2.404 (axial)	2.408 (axial)	
h-doped	Ag IS —4 + 2	Ag(III) LS —4 + 2†	Ag(III) HS —6
	2.035 (square)	1.931 (square)	2.056 (octahedron)
	1.884 (axial)	2.509 (axial)	

^aAg—F distances in angstroms. An average distance is provided for each Ag site and in some cases (indicated with †), the distances are averaged over more than one solution, in which that type of site appears. Numbers next to the species name (in bold) designate coordination numbers. LS—low spin, H—high spin, IS—intermediate spin.

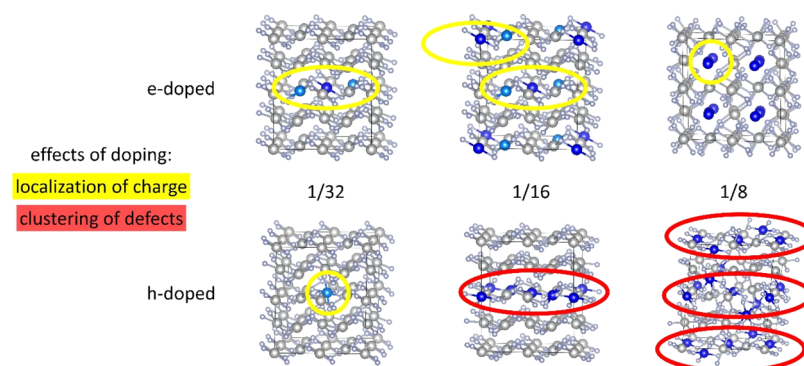


Figure 4. Illustration of charge localization and clustering of defects in doped AgF_2 polymorphs. Large gray spheres—Ag(II), blue spheres—Ag(I)/Ag(III), small gray spheres—F.

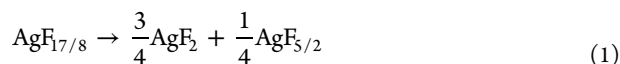
cell doubled along the *a* direction in order to test whether this solution was determined by symmetry constraints that preserve the inversion center of the unit cell. However, the result was the same, which indicates that it is the local symmetry (i.e., inversion center at the null-spin Ag(I) site) that is preserved. Finally, h-doped solution at the 1/32 level features the hole localized on a single central Ag site and its neighboring F atoms, while the 1/16 solution hosts four low-spin Ag(III) cations confined to a single AgF_2 layer.

Further insights into the influence of doping on the crystal structure of AgF_2 are provided through examination of local coordination of Ag sites (Figure 3 and Table 1). In stoichiometric (undoped) AgF_2 , all Ag sites exhibit a coordination pattern of 4 + 2 F atoms in an elongated, tilted octahedron, characteristic of Jahn–Teller-active d^9 metal cations. In doped solutions, Ag centers with an altered magnetic moment undergo a concomitant change in local coordination. The Ag(I) species in 1/32 and 1/16 e-doped solutions show an increased length of the two in-plane F contacts, with simultaneous shortening of the axial (interlayer) F contacts. In the 1/8 solution, the Ag(I) cation is surrounded by 6 or 7 F atoms at a length between ca. 2.3–2.6 Å. [Half of Ag(I) cations in this solution is coordinated in a trigonal prism pattern, and another half also picks up a seventh F atom to form a trigonal prism monocapped on one of its rectangular faces.] Such changes point to a less directional and more spherical distribution of electrons and disappearance of the first-order Jahn–Teller effect, as expected for a closed-shell (d^{10}) Ag(I) cation. In addition, the average length of F contacts is slightly larger than for Ag(II) species—a further evidence of decreased oxidation state and stronger repulsion

between atoms. These effects can, to some extent, be observed also for the intermediate-spin Ag sites in e-doped solutions at 1/32 and 1/16 levels.

On the other hand, in h-doped solutions, an approximately octahedral coordination is retained also for Ag(III) and intermediate-spin Ag sites. The former—both the high-spin and low-spin species—show an overall decrease of average Ag—F bond length [compared to Ag(II)], which is expected at their higher oxidation state. The intermediate-spin Ag site is coordinated in a pattern of a compressed tilted octahedron. The shortened Ag—F axial bonds (Table 1) can be explained by (a) the fact that these F atoms are only bonded to one Ag atom and therefore their electron cloud is redistributed to minimize repulsion and (b) their non-zero magnetic moment, indicating the partial presence of holes and thus decreased electron density.

Defect Clustering and Phase Separation. Joint analysis of structural and magnetic data points to a strong tendency of bulk AgF_2 for localization of defects resulting from doping (Figure 4). In most stable e-doped solutions, the additional charge tends to localize at particular atoms and is not distributed evenly across the unit cell. This is further supported by electron localization function (ELF) plots, which are shown in Section S5 of Supporting Information. In addition, these defects can also be clustered close to each other within a layer of AgF_2 —for example, at the 1/16 level of h-doping, all defects in the supercell are clustered within one out of four layers. This effectively leads to a structure in which three layers are undoped and one of them is 1/4-h-doped. This may indicate that such a system would in fact be unstable toward phase separation, according to the equation



where $\text{AgF}_{21/2}$ corresponds to the known fluoride of $[\text{Ag(II)F}][\text{Ag(III)F}_4]$ stoichiometry.²⁵ The calculated free energy of this reaction (eq 1) amounts to -0.06 eV per formula unit of doped AgF_2 (ca. -6 kJ/mol). This gives further credibility to the phase separation scenario for this system. Lattice constants and Ag–F bond lengths in the optimized model only differ by up to 2% from the parameters of the experimentally determined structure,²⁵ which justifies the above-mentioned energetic considerations.

As can be seen in Figure 5, the free energy of formation of doped polymorphs is positive in almost all cases, with the

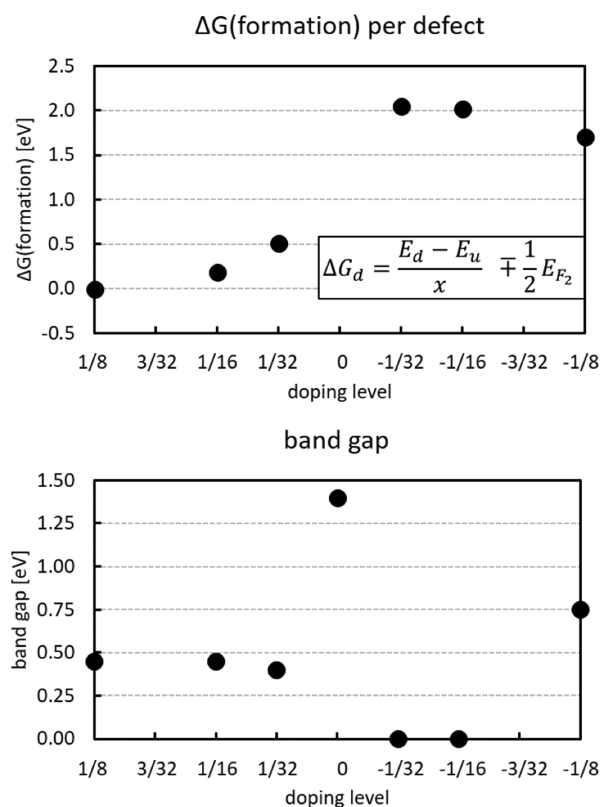


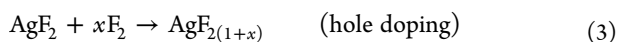
Figure 5. Energy cost and band gap of doped AgF_2 . Top panel: free energy of formation per defect (ΔG_d). Inset shows the equation for ΔG_d , where E_d and E_u are total energies of doped and undoped supercells, respectively, x is the number of added or removed F atoms, and E_{F_2} is the total energy of solid F_2 per FU. Bottom panel: band gap. On x axis, “+” represents hole doping and “−” represents electron doping.

exception of h-doping at the 1/8 level, where it is only slightly negative—equal to -0.02 eV. (Note: free energy is, in this instance, equivalent to enthalpy, as the calculations are performed at $T \rightarrow 0$ K, so the entropy term is null, and at constant pressure, formally $p \rightarrow 0$ GPa.)

The generalized reaction equations, which describe doping, are



and



Therefore, for electron doping, the equilibrium would be shifted toward products at higher temperatures, as it would increase the entropy of gaseous fluorine. According to our estimates, which are based on our results and thermochemical data for fluorine,²⁶ temperatures required for synthesis of e-doped polymorphs would amount to ca. 1300 K for the 1/8 doping level and ca. 1500 K for 1/16 and 1/32 doping levels. However, thermal decomposition of AgF_2 starts to occur at a much lower temperature—ca. 960 K (690 °C).²⁷ For this reason, such synthesis is unlikely to be successful. On the other hand, the enthalpies of formation of h-doped polymorphs are less unfavorable, and while they are expected to be more positive at higher temperatures, h-doped AgF_2 could in principle be obtained at higher F_2 pressures. Obviously, the opposite is expected to be true for e-doping.

The asymmetry between electron and hole doping in terms of energy cost is reflected in the body of knowledge about the Ag–F phase diagram, both experimental and computational. There are two known mixed-valence silver fluorides: Ag_2F_5 (or $\text{Ag}^{\text{II}}\text{F}[\text{Ag}^{\text{III}}\text{F}_4]$)²⁵ and Ag_3F_8 (or $\text{Ag}^{\text{II}}[\text{Ag}^{\text{III}}\text{F}_4]_2$).²⁸ Both compounds contain Ag(II) and Ag(III) species, and they exhibit mixed- and not intermediate-valence character, with different crystallographic sites for both types of silver cations. On the other hand, there are currently no known binary fluorides which would contain both Ag(I) and Ag(II) species, although at least one example of a ternary fluoride containing those species has been obtained.²⁹ Theoretical considerations regarding the possible stability of mixed-valence binary Ag(I)/Ag(II) fluorides have been previously published.³⁰ However, from the experience of our group and our collaborators, attempts at obtaining such compounds (which included controlled thermal decomposition of AgF_2) have, in all but two instances, led to separated phases of AgF and AgF_2 .^{31,32}

Given the insight from the structural data for undoped and doped polymorphs in this work, as well as the experimental data on silver fluorides,^{22,25,28,33} it can be noted that in terms of local coordination patterns, Ag(II) and Ag(III) species tend to be much more similar to each other than any of the two is to Ag(I). In other words, substitution of Ag(II) for Ag(III) exerts a much weaker strain on the crystal structure than its substitution for Ag(I) species. This may be the main reason for both (a) higher (more positive) energy of formation for e-doping in this work and (b) lack of Ag(I)/Ag(II) mixed-valence binary fluorides in the experimental literature.

Electronic Structure. Figure 6 shows the eDOS graphs of the obtained ground-state solutions for undoped and doped AgF_2 . For the undoped, stoichiometric case, the band gap is predominantly between occupied ligand states of F and empty metal states of Ag, making this compound a classic charge-transfer insulator according to Zaanen–Sawatzky–Allen model,³⁴ as has been shown in previous works.¹ There is also strong admixing between Ag and F states, which is attributed to strong covalence of Ag–F bonds in AgF_2 , documented in previous X-ray photoelectron spectroscopy studies of silver fluorides.³⁵ Because of these characteristics, we can expect that additional occupied states in the e-doped solutions will have a majority Ag character, while holes will be largely of F character.

Indeed, this is the case in the studied solutions. We used the previous insight from magnetic structure analysis to identify sites of Ag(II), Ag(I), and Ag(III) characters in the electronic structure. The intermediate-spin Ag cations indicated in Figure 2 were designated as Ag(I) or Ag(III). As expected, the new

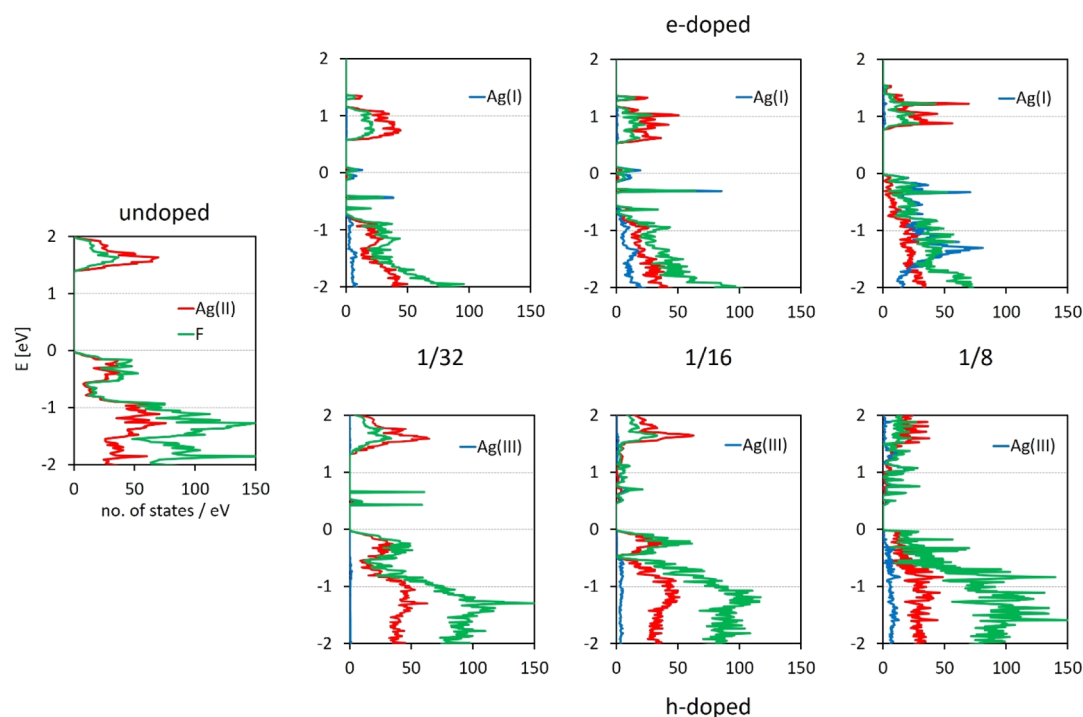


Figure 6. eDOS plots for undoped AgF_2 and for doped AgF_2 polymorphs. Zero energy corresponds to E_{Fermi} .

states appear in the former band gap. For example, at 1/32 and 1/16 levels of e-doping, the new states are predominantly of Ag(I) character and are less strongly bound, that is, at higher energy in eDOS. These new bands are very narrow, in agreement with the presence of localized Ag(I) sites in the structure. Surprisingly, some of the new Ag(I) states appear just above the Fermi level and right next to Ag(I) states below it. These empty Ag(I) states are probably an artifact related to the previously discussed symmetrical distribution of additional spin as a superposition of two solutions, as shown in Figure 2. While the calculated band gap retains a non-zero value (ca. 0.02 eV) which is smaller than the width of smearing used in eDOS calculations (0.15 eV), yet it may be artificial; it is expected to be extremely sensitive both to the doping level and to smearing and may also arise from a supercell approach. On the other hand, the new in-gap states in h-doped 1/32 and 1/16 models have a strong F contribution, which suggests that the holes are more localized on F than on Ag, and that the chemical species present in the structure is actually similar to the F^\bullet radical. At the same time, the Ag(III) states are much less pronounced. At the 1/8 level, e-doping manifests as new Ag(I) states, which are somewhat more dispersed just below the Fermi level, which also leads to a relative shift of empty Ag(II) bands and shrinking of the band gap to ca. 0.7 eV. In h-doped 1/8 solution, there are numerous, but narrow and localized states of both Ag(III) and F character (in roughly equal measure) within the former gap, effectively shrinking it to ca. 0.4 eV. Extended eDOS graphs can be found in Section S8 of Supporting Information.

The picture emerging from the analysis of crystal, magnetic, and electronic structures of doped AgF_2 polymorphs suggests a strong propensity of the system toward self-trapping of defects introduced by modification of fluorine content. In particular, at the 1/8 doping level—which is close to the optimal level of doping in cuprate-based high- T_c superconductors—localization of additional charge and reduction of the band gap,

compared to undoped AgF_2 , are observed. This is similar, indeed, to the so-called 1/8-anomaly in cuprates.³⁶

Pressure Effects. As previously mentioned, pressure is also an interesting factor to study in the case of doped AgF_2 . Increased pressure usually leads to broadening of electronic bands and eventually metallization because of increased orbital overlap induced by shorter interatomic distances.³⁷ Pressure is also an important factor impacting the T_c in oxygen-doped cuprates, which usually exhibit a maximum of T_c in their phase diagram while at optimum external pressure.^{38–41} Similar effects might be envisaged for the doped AgF_2 . Because AgF_2 is known to undergo a drastic structural reorganization into a nanotubular polymorph at ca. 14 GPa,⁴² we decided to study only the range up to 10 GPa, as the second-order transition at ca. 7 GPa leads only to a slight symmetry lowering.²¹ The selected data are presented for e-doping in Figure 7 and h-doping in Figure 8. In the case of e-doping, the increase of formation energy with pressure is apparent (Figure 7, top) because of factors described above; namely, the equilibrium is shifted toward substrates, which consist only of AgF_2 and thus have lower volume (eq 2). The band gap (Figure 7, top) remains virtually unaffected for polymorphs at 1/8 and 1/32 levels of e-doping. However, the polymorph at the 1/16 doping level undergoes an electronic and structural transition between 7.5 and 10.0 GPa into a polymorph similar to the one found at the 1/8 doping level (Figure 7, middle): the band gap becomes wide open again and equal to ca. 0.7 eV, and the Ag(I) cations are aligned in channels roughly along the c direction and with the distance to F atoms on average ca. 0.2 Å larger for the remaining Ag(II) cations. It appears, therefore, that doped AgF_2 resists metallization by rearranging the vacancies and opening the band gap, which is in line with generalized maximum hardness principle.⁴³ More detailed documentation of this process in e-doped AgF_2 can be found in Section S7 of Supporting Information.

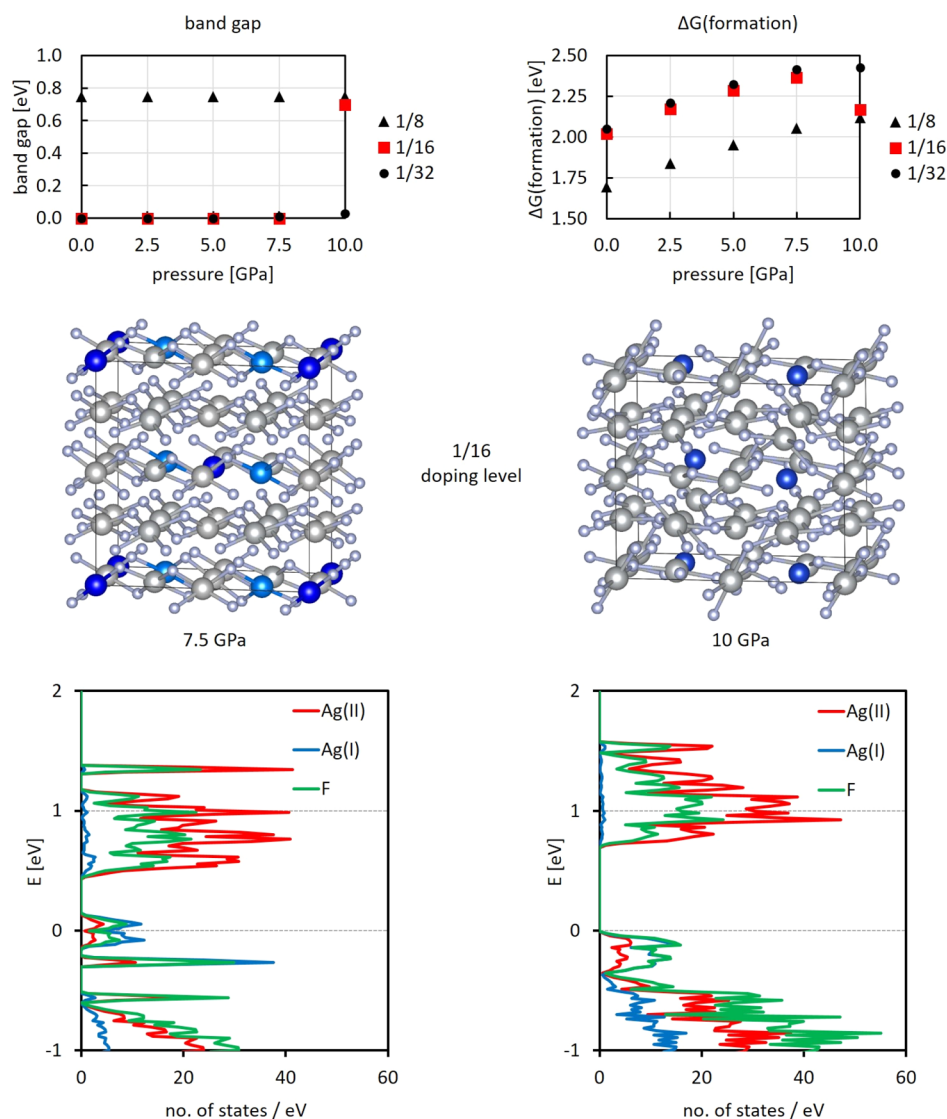


Figure 7. Pressure effects in e-doped AgF_2 . Top panel: band gap and free energy of formation; middle panel: comparison of 1/16 e-doped structures before and after phase transition; bottom panel: eDOS graphs for 1/16 e-doped structures before and after phase transition.

In the case of h-doped AgF_2 , as predicted above, the free energy of formation mostly decreases with pressure (Figure 8, top). The most noticeable process observed here is the transition of the h-doped structure at the 1/32 level between 7.5 and 10 GPa, which leads to redistribution of charge and spin: the single, intermediate-spin Ag site in the center of the unit cell is replaced by two high-spin Ag(III) cations—one in the center and another one on the *ab* wall of the unit cell (Figure 8, middle). As in the 1/8 h-doped solution, these high-spin Ag(III) species are coordinated by six F atoms at an average distance of 2.06 Å (compared to the compressed octahedral pattern of the intermediate-spin Ag center at lower pressure; see also Table 1). This transition is most likely second-order, as there are no corresponding discontinuities in the pressure dependence of volume and lattice constants (cf. Section S6 of Supporting Information). This process increases the band gap to ca. 0.25 eV, which was previously reduced in the 0–7.5 GPa range from 0.4 to 0.15 eV (Figure 8, bottom). A nonmonotonic pressure dependence of the band gap and free energy of formation is also notable for the 1/8 solution (Figure 8, top). However, the dependence of cell volume and

vectors is monotonic within the studied range and there are no discernible structural modifications. Most likely, this behavior stems from the presence of a variety of electronic states (high- and low-spin Ag(III), holes on F) in the first place, which respond to increasing pressure in different ways.

CONCLUSIONS

Our computational studies of chemical doping of AgF_2 indicate that (a) electron- and hole-doped AgF_2 remains—for the most part—insulating and resistant to metallization by pressure up to 10 GPa; (b) the additional electronic states arising upon doping are highly localized; and (c) the spatial distribution of defects in the unit cell of lowest-energy solutions suggests propensity of the system toward phase separation. Such results seem to indicate that chemical doping to AgF_2 is nearly impossible—as far as the conditions of thermodynamic equilibrium are assumed. In our recent study of polarons in AgF_2 , lattice self-trapping of defects induced by the modified electron count in the unit cell was also observed for bulk AgF_2 —but, importantly, to a lesser extent in hypothetical polymorphs with flat monolayers.⁶ This is also in line with

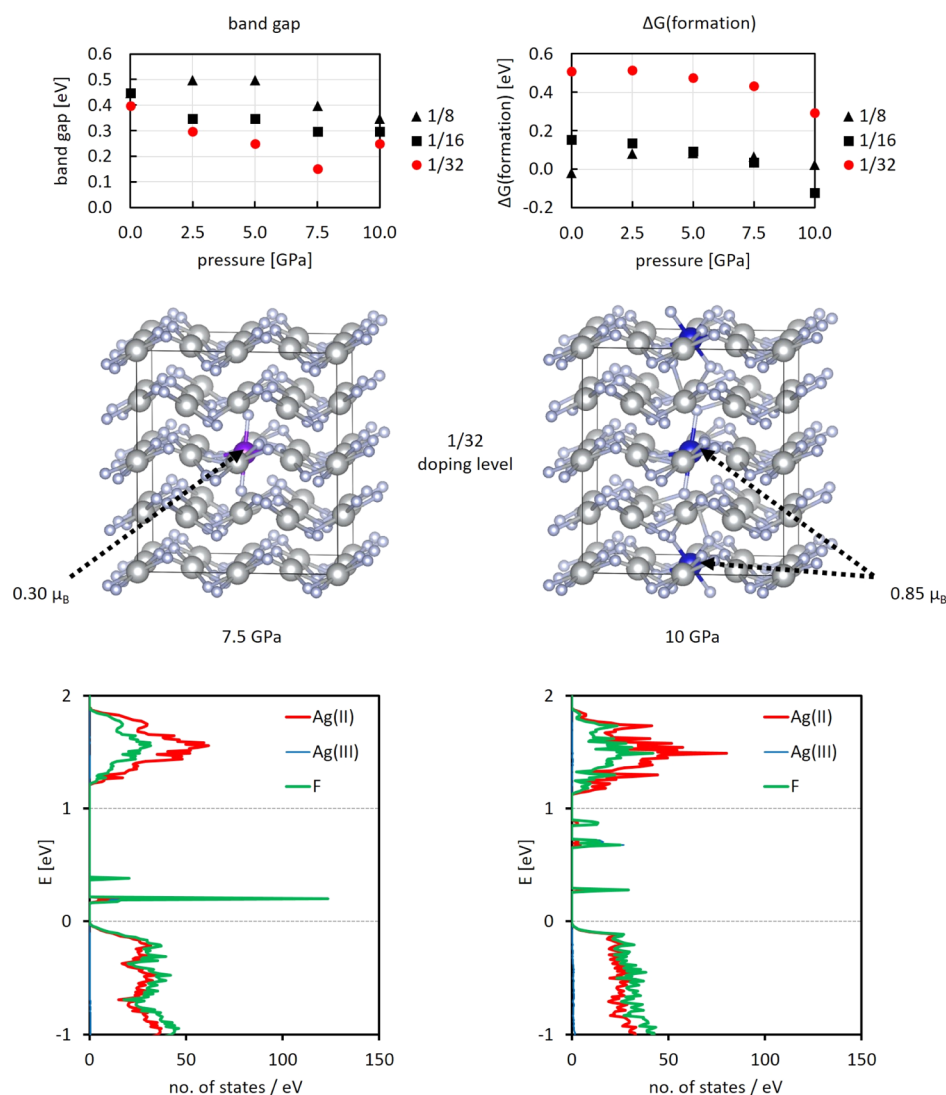


Figure 8. Pressure effects in h-doped AgF_2 . Top panel: band gap and free energy of formation; middle panel: comparison of 1/32 h-doped structures before and after phase transition; bottom panel: eDOS graphs for 1/32 h-doped structures before and after phase transition.

strong covalence of Ag–F bonds, well documented in previous studies,³⁵ which leads to strong vibronic coupling and in turn increases the tendency for trapping of defects. Another thing to consider is that the type of doping studied here, while in principle similar to chemical modifications of cuprates, is by definition more local: the fluorine defects/interstitials ultimately have to occupy a particular position in the unit cell, different from any of the original F atoms in the stoichiometric AgF_2 because of symmetry constraints (or rather, the appearance of the said modifications breaks some of those constraints). In cuprates, doping is usually achieved by substitution of a fraction of closed-shell cations for isoelectronic cations with different oxidation states, and while this is often associated with oxygen deficiency, these modifications ultimately exert a much weaker structural influence on the resulting compound. AgF_2 , while a direct analogue to La_2CuO_4 in many ways, is a binary rather than ternary compound, which makes such substitutions at the La site impossible. Given all of the above, chemical doping of AgF_2 , even combined with application of external pressure, is unlikely to produce materials with properties that could be promising from the point of view of high-temperature

superconductivity. Our conclusions reached here using “chemical” models are worth to be compared to a parallel study on polaronic states in stoichiometric AgF_2 polytypes using external charge doping.⁶

Moreover, there are also different pathways toward cuprate-like properties in AgF_2 that are currently being explored—in particular, a flat AgF_2 monolayer stabilized and doped by using an appropriate substrate for epitaxy.⁷ In addition, because our models always contain the inversion center and because we discuss only the lowest energy solutions, it is not improbable that in the real-life experiment, some metastable metallic structures could be obtained (cf. Section S9 in the Supporting Information). In other words, one may search for doped AgF_2 in the conditions far from the thermodynamic equilibrium; indeed, two of the higher-energy structures found in this work are predicted to exhibit metallic DOS (Section S9 in Supporting Information).

■ ASSOCIATED CONTENT

Supporting Information

The Supporting Information is available free of charge at <https://pubs.acs.org/doi/10.1021/acs.inorgchem.0c02970>.

Structural data on input doped models, electronic structure of selected doped solutions for different values of Hubbard U , electronic structure of e^- - and h -doped cuprates calculated with the GGA + U approach, spin density maps for ground-state doped solutions, ELF maps for selected ground-state doped solutions, pressure dependence of lattice parameters for doped AgF_2 polymorphs, resistance of e -doped AgF_2 to metallization, expanded eDOS graphs, selected higher-energy solutions, and structure of an undoped AgF_2 supercell (PDF)

AUTHOR INFORMATION

Corresponding Authors

Adam Grzelak – Center of New Technologies, University of Warsaw, 02-097 Warsaw, Poland; orcid.org/0000-0003-4707-3031; Email: a.grzelak@cent.uw.edu.pl

Wojciech Grochala – Center of New Technologies, University of Warsaw, 02-097 Warsaw, Poland; orcid.org/0000-0001-7317-5547; Email: w.grochala@cent.uw.edu.pl

Author

Mariana Derzsi – Center of New Technologies, University of Warsaw, 02-097 Warsaw, Poland; Advanced Technologies Research Institute, Faculty of Materials Science and Technology in Trnava, Slovak University of Technology in Bratislava, 917 24 Trnava, Slovakia

Complete contact information is available at:
<https://pubs.acs.org/10.1021/acs.inorgchem.0c02970>

Notes

The authors declare no competing financial interest.

ACKNOWLEDGMENTS

W.G. thanks the Polish National Science Center (NCN) for the Maestro project (2017/26/A/ST5/00570). This research was carried out with the support of the Interdisciplinary Centre for Mathematical and Computational Modelling (ICM), University of Warsaw under grant ADVANCE++ (no. GA76-19). M.D. acknowledges the ERDF fund, Research and Innovation Operational Programme (ITMS2014+: 313011W085), Scientific Grant Agency of the Slovak Republic (VG 1/0223/19), and the Slovak Research and Development Agency (APVV-18-0168).

DEDICATION

This work is dedicated to Prof. Boris Žemva on his 80th birthday.

REFERENCES

- Gawraczyński, J.; Kurzydłowski, D.; Ewings, R. A.; Bandaru, S.; Gadamski, W.; Mazej, Z.; Ruani, G.; Bergenti, L.; Jaroń, T.; Ozarowski, A.; Hill, S.; Leszczyński, P. J.; Tokár, K.; Derzsi, M.; Barone, P.; Wohlfeld, K.; Lorenzana, J.; Grochala, W. Silver Route to Cuprate Analogs. *Proc. Natl. Acad. Sci. U.S.A.* **2019**, *116*, 1495–1500.
- Miller, C.; Botana, A. S. Cupratelike Electronic and Magnetic Properties of Layered Transition-Metal Difluorides from First-Principles Calculations. *Phys. Rev. B* **2020**, *101*, 195116.
- Kurzydłowski, D.; Grochala, W. Prediction of Extremely Strong Antiferromagnetic Superexchange in Silver(II) Fluorides: Challenging the Oxocuprates(II). *Angew. Chem., Int. Ed.* **2017**, *56*, 10114–10117.
- Pickett, W. E. Electronic Structure of the High-Temperature Oxide Superconductors. *Rev. Mod. Phys.* **1989**, *61*, 433–512.

- Ahn, C. H.; Bhattacharya, A.; Di Ventura, M.; Eckstein, J. N.; Frisbie, C. D.; Gershenson, M. E.; Goldman, A. M.; Inoue, I. H.; Mannhart, J.; Millis, A. J.; Morpurgo, A. F.; Natelson, D.; Triscone, J.-M. Electrostatic Modification of Novel Materials. *Rev. Mod. Phys.* **2006**, *78*, 1185–1212.

- Bandaru, S.; Derzsi, M.; Grzelak, A.; Lorenzana, J.; Grochala, W. Fate of Doped Carriers in Silver Fluoride Cuprate Analogues. *Phys. Rev. Lett.* **2021**, submitted for publication.

- Grzelak, A.; Su, H.; Yang, X.; Kurzydłowski, D.; Lorenzana, J.; Grochala, W. Epitaxial Engineering of Flat Silver Fluoride Cuprate Analogs. *Phys. Rev. Mater.* **2020**, *4*, 084405.

- Bednorz, J. G.; Müller, K. A. Possible High T_c Superconductivity in the Ba-La-Cu-O System. *Z. Phys. B: Condens. Matter* **1986**, *64*, 189–193.

- Al-Mamouri, M.; Edwards, P. P.; Greaves, C.; Slaski, M. Synthesis and Superconducting Properties of the Strontium Copper Oxy-Fluoride $\text{Sr}_2\text{CuO}_2\text{F}_{2+\delta}$. *Nature* **1994**, *369*, 382–384.

- Kresse, G.; Hafner, J. Ab Initio Molecular Dynamics for Liquid Metals. *Phys. Rev. B: Condens. Matter Mater. Phys.* **1993**, *47*, 558–561.

- Kresse, G.; Hafner, J. Ab Initio Molecular-Dynamics Simulation of the Liquid-Metalamorphous-Semiconductor Transition in Germanium. *Phys. Rev. B: Condens. Matter Mater. Phys.* **1994**, *49*, 14251–14269.

- Kresse, G.; Furthmüller, J. Efficiency of Ab-Initio Total Energy Calculations for Metals and Semiconductors Using a Plane-Wave Basis Set. *Comput. Mater. Sci.* **1996**, *6*, 15–50.

- Kresse, G.; Furthmüller, J. Efficient Iterative Schemes for Ab Initio Total-Energy Calculations Using a Plane-Wave Basis Set. *Phys. Rev. B: Condens. Matter Mater. Phys.* **1996**, *54*, 11169–11186.

- Kresse, G.; Joubert, D. From Ultrasoft Pseudopotentials to the Projector Augmented-Wave Method. *Phys. Rev. B: Condens. Matter Mater. Phys.* **1999**, *59*, 1758–1775.

- Perdew, J. P.; Ruzsinszky, A.; Csonka, G.; Vydrov, O.; Scuseria, G.; Constantin, L.; Zhou, X.; Burke, K. Restoring the Density-Gradient Expansion for Exchange in Solids and Surfaces. *Phys. Rev. Lett.* **2008**, *100*, 136406.

- Liechtenstein, A. I.; Anisimov, V. I.; Zaanen, J. Density-Functional Theory and Strong Interactions: Orbital Ordering in Mott-Hubbard Insulators. *Phys. Rev. B: Condens. Matter Mater. Phys.* **1995**, *52*, R5467–R5470.

- Kasinathan, D.; Kyker, A. B.; Singh, D. J. Origin of Ferromagnetism in Cs_2AgF_4 : The Importance of Ag-F Covalency. *Phys. Rev. B: Condens. Matter Mater. Phys.* **2006**, *73*, 214420.

- Momma, K.; Izumi, F. VESTA 3 for Three-Dimensional Visualization of Crystal, Volumetric and Morphology Data. *J. Appl. Crystallogr.* **2011**, *44*, 1272–1276.

- Dubay, O. *p4vasp*, 2017

- Freysoldt, C.; Grabowski, B.; Hickel, T.; Neugebauer, J.; Kresse, G.; Janotti, A.; Van De Walle, C. G. First-Principles Calculations for Point Defects in Solids. *Rev. Mod. Phys.* **2014**, *86*, 253–305.

- Grzelak, A.; Gawraczyński, J.; Jaroń, T.; Kurzydłowski, D.; Budzianowski, A.; Mazej, Z.; Leszczyński, P. J.; Prakash, V. B.; Derzsi, M.; Struzhkin, V. V.; Grochala, W. High-Pressure Behavior of Silver Fluorides up to 40 GPa. *Inorg. Chem.* **2017**, *56*, 14651–14661.

- Fischer, P.; Roullet, G.; Schwarzenbach, D. Crystal and Magnetic Structure of Silver Difluoride-II. Weak 4d-Ferromagnetism of AgF_2 . *J. Phys. Chem. Solids* **1971**, *32*, 1641–1647.

- Goodenough, J. B. An Interpretation of the Magnetic Properties of the Perovskite-Type Mixed Crystals $\text{La}_{1-x}\text{Sr}_x\text{CoO}_{3-\delta}$. *J. Phys. Chem. Solids* **1958**, *6*, 287–297.

- Jaroń, T.; Grochala, W. Prediction of Giant Antiferromagnetic Coupling in Exotic Fluorides of Ag. *Phys. Status Solidi RRL* **2008**, *2*, 71–73.

- Fischer, R.; Müller, B. G. Die Kristallstruktur von $\text{Ag}^{\text{II}}\text{F}-[\text{Ag}^{\text{III}}\text{F}_4]$. *Z. Anorg. Allg. Chem.* **2002**, *628*, 2592–2596.

- Chase, M. W. *NIST-JANAF Thermochemical Tables*, 4th ed.; National Institute of Standards and Technology: Gaithersburg, MD, U. S. A, 1998.

(27) Grochala, W. Greedy Ag(II) Oxidizer: Can Any Inorganic Ligand except Fluoride Endure Its Presence in Ionic Solids? *J. Fluorine Chem.* **2008**, *129*, 82–90.

(28) Graudejus, O.; Wilkinson, A. P.; Bartlett, N. Structural Features of Ag[AuF₄] and Ag[AuF₆] and the Structural Relationship of Ag[AgF₄]₂ and Au[AuF₄]₂ to Ag[AuF₄]₂. *Inorg. Chem.* **2000**, *39*, 1545–1548.

(29) Mazej, Z.; Michalowski, T.; Goresnik, E. A.; Jagličić, Z.; Arčon, I.; Szydłowska, J.; Grochala, W. The First Example of a Mixed Valence Ternary Compound of Silver with Random Distribution of Ag^I and Ag^{II} Cations. *Dalton Trans.* **2015**, *44*, 10957–10968.

(30) Grochala, W. On Possible Existence of Pseudobinary Mixed Valence Fluorides of Ag(I) / Ag(II): A DFT Study. *J. Mol. Model.* **2011**, *17*, 2237–2248.

(31) Mazej, Z. Jožef Stefan Institute, Ljubljana, Slovenia. Private communication, **2020**.

(32) Gawraczyński, J. Optical Spectroscopy of Selected Divalent Silver Compounds. Doctoral Thesis, University of Warsaw, 2019.

(33) Žemva, B.; Lutar, K.; Jesih, A.; Casteel, W. J.; Wilkinson, A. P.; Cox, D. E.; Von Dreele, R. B.; Borrmann, H.; Bartlett, N. Silver Trifluoride: Preparation, Crystal Structure, Some Properties, and Comparison with AuF₃. *J. Am. Chem. Soc.* **1991**, *113*, 4192–4198.

(34) Zaanen, J.; Sawatzky, G. A.; Allen, J. W. Band Gaps and Electronic Structure of Transition-Metal Compounds. *Phys. Rev. Lett.* **1985**, *55*, 418–421.

(35) Grochala, W.; Egdell, R. G.; Edwards, P. P.; Mazej, Z.; Žemva, B. On the Covalency of Silver-Fluorine Bonds in Compounds of Silver(I), Silver(II) and Silver(III). *ChemPhysChem* **2003**, *4*, 997–1001.

(36) Feng, D. L.; Shen, Z.-X.; Zhou, X. J.; Shen, K. M.; Lu, D. H.; Marel, D. V. D. Puzzles about 1/8 Magic Doping in Cuprate. *J. Phys. Chem. Solids* **2006**, *67*, 198–200.

(37) Grochala, W.; Hoffmann, R.; Feng, J.; Ashcroft, N. W. The Chemical Imagination at Work in Very Tight Places. *Angew. Chem., Int. Ed.* **2007**, *46*, 3620–3642.

(38) Chen, X. J.; Struzhkin, V. V.; Hemley, R. J.; Mao, H. K.; Kendziora, C. High-Pressure Phase Diagram of Bi₂Sr₂CaCu₂O_{8+δ} Single Crystals. *Phys. Rev. B: Condens. Matter Mater. Phys.* **2004**, *70*, 214502.

(39) Chen, X.-J.; Struzhkin, V. V.; Yu, Y.; Goncharov, A. F.; Lin, C.-T.; Mao, H.-k.; Hemley, R. J. Enhancement of Superconductivity by Pressure-Driven Competition in Electronic Order. *Nature* **2010**, *466*, 950–953.

(40) Zhang, J.-B.; Struzhkin, V. V.; Yang, W.; Mao, H.-K.; Lin, H.-Q.; Ma, Y.-C.; Wang, N.-L.; Chen, X.-J. Effects of Pressure and Distortion on Superconductivity in Tl₂Ba₂CaCu₂O_{8+δ}. *J. Phys.: Condens. Matter* **2015**, *27*, 445701.

(41) Struzhkin, V. V.; Chen, X.-J. Magnon-Phonon Coupling and Implications for Charge-Density Wave States and Superconductivity in Cuprates. *Low Temp. Phys.* **2016**, *42*, 884–890.

(42) Grzelak, A.; Gawraczyński, J.; Jaroń, T.; Kurzydłowski, D.; Mazej, Z.; Leszczyński, P. J.; Prakapenka, V. B.; Derzsi, M.; Struzhkin, V. V.; Grochala, W. Metal Fluoride Nanotubes Featuring Square-Planar Building Blocks in a High-Pressure Polymorph of AgF₂. *Dalton Trans.* **2017**, *46*, 14742–14745.

(43) Grochala, W. The Generalized Maximum Hardness Principle Revisited and Applied to Solids (Part 2). *Phys. Chem. Chem. Phys.* **2017**, *19*, 30984–31006.